Quantum Electronics **50** (11) 1015–1022 (2020)

LASER SPECTROSCOPY OF ATOMS

https://doi.org/10.1070/QEL17433

Two-frequency sub-Doppler spectroscopy of the caesium D_1 line in various configurations of counterpropagating laser beams

D.V. Brazhnikov, S.M. Ignatovich, I.S. Mesenzova, A.M. Mikhailov, R. Boudot, M.N. Skvortsov

Abstract. **Sub-Doppler resonances in caesium vapours are studied in a laser field produced by counterpropagating two-frequency light beams with mutually orthogonal linear polarisations. The beams are in resonance with optical transitions in the D_1 line, the frequency difference of the field spectral components being equal to the hyperfine ground-state splitting in the Cs atom (~9.2 GHz). It has already been shown that in this configuration, the hypercontrast effect can be observed for sub-Doppler resonances, which makes this configuration promising for the employment in new-generation miniature optical frequency standards. In the present work, two different two-frequency configurations are compared with each other and with the single-frequency configuration widely used in practice for observing saturated absorption resonances. The parameters of nonlinear resonances are measured at various temperatures of caesium vapours and at different optical field intensities. The results of the investigations performed make it possible to find an optimal two-frequency scheme for exciting nonlinear resonances and to estimate a potential of the scheme for its applications in quantum metrology.**

Keywords: *optical frequency standards, ultra-high resolution spectroscopy, coherent population trapping, caesium, diode lasers, modulation of laser radiation.*

1. Introduction

Quantum frequency standards (QFS's) and atomic clocks on their basis have been actively developing for more than half of the century and find numerous applications in applied and fundamental physics [1]. In applied physics, QFS's can be used in satellite and inertial navigation systems, communication systems and broadband internet, in smart grids, and for synchronising signals in such important direction of astronomy and astrophysics as the very-long-baseline radio-interferometry, which yielded a series of important scientific discoveries in recent years (see, for example, [2]). In fundamental physics, QFS's are involved in various precision measurements, for example, studies of fundamental constants [3], search for dark matter [4], relativistic geodesy [5] and so on.

Apart from QFS metrological characteristics such as the relative frequency instability and accuracy, also important in many applications are dimensions, mass, and power consumption of the whole device. Evidently, the most accurate and stable are stationary arranged laboratory QFS's with an electric power consumption of, as a rule, much greater than 1 kW. Most advanced versions of such standards are based on laser-cooled atoms and ions [6–8]. The development of transportable QFS's is also important not only in solving various applied problems, but also in fundamental physics. For example, active studying of the gravitation influence on clock operation in earth conditions predicted by the general relativity theory has started with the appearance of first high-precision transportable atom clocks based on a microwave QFS with a beam of caesium atoms (Hafele–Keating experiment [9]). Presently, even more precise measurements of this effect are taken with transportable QFS's in the optical range [10]. The principle of operation of such QFS's, similarly to their laboratory analogues, may be based on using ultra-cold atoms or ions [5, 10, 11] or on the more 'classical' laser technology related to saturated absorption resonances in molecular and atomic gases (see, for example, [12–15]).

Compact versions of transportable QFS's are quite in demand and employed in onboard aircraft devices including satellites. Now, there are several technologies for creating such standards. The most compact (miniature) QFS's have a volume of less than 100 cm^3 and are based on the phenomenon of coherent population trapping (CPT) [16]. In these devices, CPT appears as a narrow nonlinear resonance in cells filled with vapours of alkali-metal atoms (Rb or Cs). The nonlinear resonance is excited by using a multi-frequency laser emission obtained in a result of the microwave modulation of the pump current of a vertical-cavity surface-emitting laser (VCSEL). A CPT resonance is used as a reference for stabilising the frequency of a microwave oscillator (μ-oscillator). Thus, CPT-based QFS's are standards in the microwave frequency range. Among the latest achievements in the field of QFS-CTP, it is worth noting, for example, papers [17–19] (see also a review [20]). In particular, the total QFS volume in [17] was only 15 cm^3 at an power consumption of about 60 mW, and the relative frequency instability (Allan deviation σ_y) was 7×10^{-11} at an averaging time of 1 s and 2×10^{-12} at 24 h. It is expected that in the near future such QFS's will provide a noticeable progress in many technologies related to the employment of mobile high-precision clocks. For example, the projects are realised in which QFS-CPT are

D.V. Brazhnikov Institute of Laser Physics, Siberian Branch, Russian Academy of Sciences, prosp. Akad. Lavrent'eva 15B, 630090 Novosibirsk, Russia; Novosibirsk State University, ul. Pirogova 1, 630090 Novosibirsk, Russia; e-mail: brazhnikov@laser.nsc.ru;
S.M. Ignatovich, I.S. Mesenzova, A.M. Mikhailov, M.N. Skvortsov Institute of Laser Physics, Siberian Branch, Russian Academy of Sciences, prosp. Akad. Lavrent'eva 15B, 630090 Novosibirsk, Russia; e-mail: sign@laser.nsc.ru;
R. Boudot FEMTO-ST, CNRS, University Bourgogne Franche-Comté, 26 rue de l'épitaphe, 25000 Besançon, France; e-mail: rodolphe.boudot@femto-st.fr

Received 4 September 2020
Kvantovaya Elektronika **50** (11) 1015–1022 (2020)
Translated by N.A. Raspopov

used for refining navigation principles in deep space with the employment of small satellites, namely CubeSats [21].

Until recently, samples of miniature QFS's only operated in the microwave range. However, the development of such QFS's in the optical range is valuable in itself. Indeed, in addition to the employment of such frequency standards as a basis for new-generation miniature optical clocks, they may be high-stability sources of laser radiation and be included in more sophisticated quantum devices, i.e. transportable atomic interferometric sensors of gravitation, acceleration, and rotation, which are now rapidly developing [22]. The first miniature optical-range QFS's competitive with respect to advanced microwave analogues have been demonstrated only in the last three years by a group of US scientists [23, 24]. The latter paper demonstrated the relative frequency stability of the developed standard $\sigma_y = 2.9 \times 10^{-12}$ at 1 s, the total QFS volume being 35 cm^3.

Importantly, in developing a miniature QFS the main problem is to find the optimal method of laser spectroscopy capable of demonstrating good results with micro-cells of volume ~10 mm^3. In particular, operation of the developed QFS [23, 24] bases on the method of two-photon spectroscopy of ^{87}Rb atoms placed in a micro-cell of size $3 \times 3 \times 3$ mm.

The authors of Refs [25, 26] proposed an alternative approach to the formation of a reference optical resonance for stabilising the laser radiation frequency. In particular, the cell filled with vapours of Cs atoms was irradiated by a field of counterpropagating laser beams, each of those having two frequency components ω_1 and ω_2, which matched the corresponding dipole transitions in the D_1 line. Here, the difference $\omega_1 - \omega_2$ is equal to the value of hyperfine splitting of the ground state ($\Delta_g \approx 2\pi \times 9.2$ GHz, Fig. 1). The frequency components ω_1 and ω_2 of the field (sidebands of the ± 1 orders) were obtained from the initial (carrying) laser frequency ω_0 by using an electro-optical modulator (EOM). In scanning frequency ω_0, the high-contrast nonlinear (sub-Doppler) resonance was obtained in an absorbing cell, which was a reference for stabilising the optical frequency. Physical reasons for a high contrast of the nonlinear resonance are thoroughly studied in [26, 27]. In [26], the optical frequency of a diode laser was stabilised by using a caesium micro-cell of approximately the same volume as in the work of American counterparts [24]. Already in first experiments, the measured relative frequency stability was $\sigma_y = 2 \times 10^{-12}$ at 1 s, which is one of the best results to date in the optical range with the employment of micro-cells.

Thus, the method of bichromatic sub-Doppler spectroscopy suggested in [25, 26] is rather promising for the employment in quantum metrology and laser physics. However, there are important issues that require an additional study. In particular, in the present work we study two different schemes for forming the laser field in a cell. In the first scheme, the laser beam is formed by simply reflecting the initial beam by a mirror back to the cell. In the second scheme, the initial beam is split into two beams: freely speaking, to the pump beam and probe beam, which pass to a glass cell through the opposite faces. For comparing nonlinear resonance characteristics of these two schemes we, similarly to other authors, introduce into consideration and study the quality parameter of a nonlinear resonance Q, which determines the short-term stability of the QFS (σ_y at 1 s). This parameter has been measured for various optical field powers in the cell at various temperatures of the latter. Results obtained are compared to those for the widely used single-frequency configuration, in which a 'conventional' resonance of saturated absorption is observed. The study conducted substantially expands the data obtained in [25–27] and allows one to discuss the optimal optical scheme and physical conditions for using the two-frequency spectroscopy method in quantum metrology.

2. Two-frequency spectroscopy method

2.1. Scheme with backward reflection from a mirror

Figure 2 presents a schematic of the experimental setup where the counterpropagating laser beam is formed by a reflected initial laser beam, which propagates along the z axis from highly reflecting mirror M arranged on a linear translation stage. This simple approach to the formation of counterpropagating laser beams in a cell was used in all previous works on this subject [25–27]. Necessity of using the stage is explained

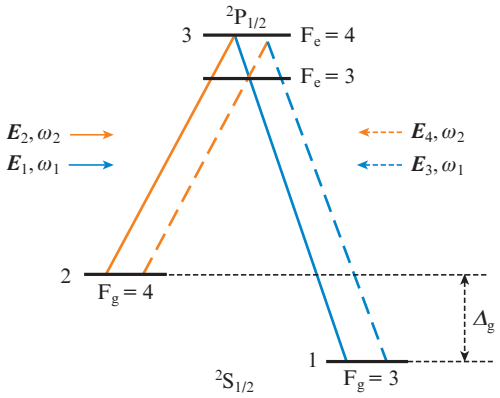

Figure 1. Energy level diagram of the D_1 line of the caesium atom. For simplicity, level degeneration in magnetic (Zeeman) sublevels m is omitted. The counterpropagating two-frequency laser beams are in resonance with the dipole transitions $F_g = 3 \rightarrow F_e = 4$ and $F_g = 4 \rightarrow F_e = 4$, the corresponding energy levels are marked with digits 1, 2, and 3. Vectors $\boldsymbol{E}_i$ ($i = 1-4$) are the real amplitudes of the corresponding travelling waves.

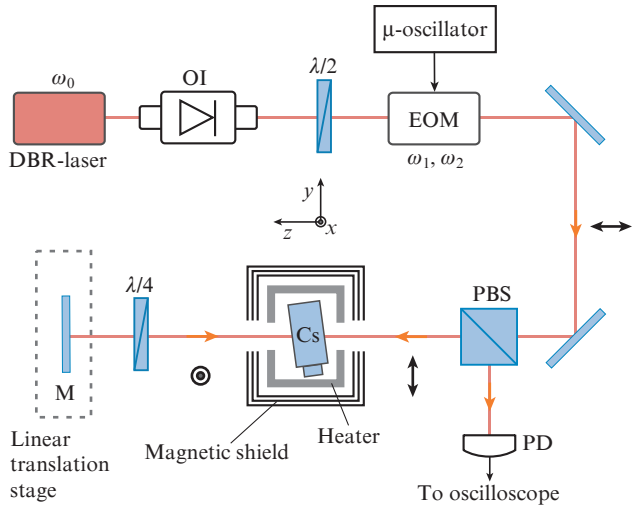

Figure 2. Experimental setup with the initial laser beam reflected by a mirror back to the cell.

by that the distance between the mirror and cell should be chosen to provide the maximal amplitude of a sub-Doppler resonance. The dependence of the resonance amplitude on this distance is thoroughly discussed in [26, 27], and we will not consider it. Note only that an oscillation of the resonance amplitude during stage motion along the z axis is the manifestation of CPT, which is related to excitation of the microwave coherent states in the caesium atom as superpositions of the magnetic sublevels pertaining to different hyperfine ground-state components $F_g = 3$ and $F_g = 4$ (see Fig. 1).

A diode DBR laser (a laser with a distributed Bragg reflector) with an emission wavelength of about 894.6 nm and a linewidth of ~1 MHz is used as a radiation source. The laser radiation passed through optical isolator OI and a half-wave plate is directed to the amplitude EOM (iXBlue NIR-MX950-LN-20) coupled to a polarisation-maintaining fibre. The EOM is fabricated by the Mach–Zehnder interferometer scheme, which provides at its output the observation of only two spectrum components with the frequencies ω_1 and ω_2 (side bands of ±1 orders) with a suppressed carrying frequency ω_0. Here, the frequency difference is $\omega_1 - \omega_2 = 4\pi f_\mu$, where f_μ is provided by a microwave μ-oscillator connected to the EOM. In all experiments with the two-frequency spectroscopy method, the frequency is $f_\mu = \Delta_g/4\pi \approx 4.6$ GHz, that is, half the value of hyperfine splitting for the ground state in the caesium atom (see Fig. 1). Under this condition, two optical transitions in the atom are excited simultaneously, which may lead to their destructive interference and CPT [28].

The laser beam of diameter ~1 mm having passed the EOM and a polarisation beam splitter PBS, is directed to a cell with vapours of caesium atoms. The cell is installed at a small angle in order to avoid undesirable backward reflections. In all the experiments, the same cylindrical cell is used with a length of 5 mm and a diameter of 20 mm fabricated from borosilicate glass. The cell is placed inside a copper heating case and a three-layer cylindrical magnetic shield made of permalloy (the shield length is 25 cm, no end-caps). The residual magnetic field measured at the cell position was not above 0.5 mG. Having passed the cell, the laser beam reflects from mirror M and passes twice (forward and backward) a quarter-wave plate $\lambda/4$, which results in a turn of the radiation initial linear polarisation by 90°. After the second passage through the cell, the laser beam is directed to a photodetector PD, whose signal is analysed by an oscilloscope as a function of the laser frequency ω_0.

Thus, the laser field configuration is formed in a cell, which comprises counterpropagating bichromatic laser beams with orthogonal linear polarisations. As shown in [25–27], the sub-Doppler resonance is observed in such a configuration in the form of homogeneously broadened dip in a power of the radiation passed through the cell. It can be termed 'the inverse resonance of saturated absorption'. An example of such a resonance is shown in Fig. 3. On the abscissa the laser frequency detuning from the average frequency of two optical transitions is plotted $\delta_0 = \omega_0 - (\omega_{31} + \omega_{32})/2$, where ω_{ij} are the frequencies of the corresponding optical transitions (see Fig. 1). The ordinate is a signal of the photodetector PD. The dashed slanting line in Fig. 3 refers to the total passage of the light beam without absorption in the cell (laser frequency ω_0 was tuned by varying the laser pump current, which explains the deviation of this line from horizontal and the absorption profile asymmetry). In the experiments (with the current and following configurations) the laser beam power P was measured prior to PBS.

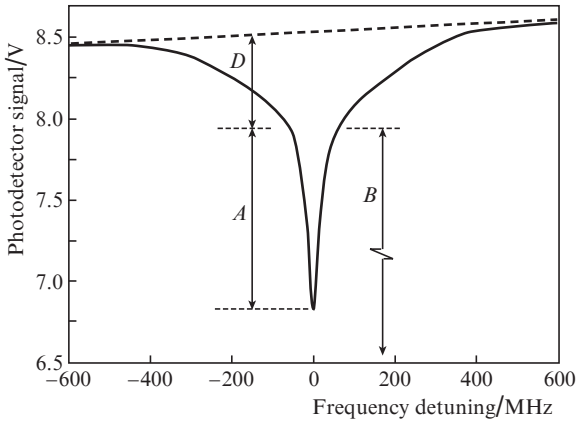

Figure 3. Sub-Doppler spectroscopy of caesium atoms in the field of counterpropagating two-frequency laser beams at $T \approx 42$ °C, $P \approx 1.5$ mW; A, B, and D are the amplitudes of the central resonance, background signal, and Doppler profile, respectively.

Note that a conventional resonance of saturated absorption observed in the single-frequency scheme with the waves of similar polarisations, as a rule, increases transmission at the resonance centre. In our case, the resonance has an opposite sign: a noticeably increased absorption is observed at the profile centre. Such an inversion of the sign of sub-Doppler resonance in not surprising. Indeed, an inverted resonance of this kind have been observed earlier in various configurations of light fields (see, for example, [29–32]). However, a distinctive feature of the two-frequency scheme used is the contrast value of the nonlinear signal: the central resonance amplitude A may substantially exceed that of a wide Doppler profile D (Fig. 3). In the case of a conventional resonance of saturated absorption this amplitude is, as a rule, not above 20%–30% of the Doppler profile amplitude (see, for example, [14, 33, 34], and Section 3 of the present paper). In the case shown in Fig. 3, the amplitude of the sub-Doppler resonance is approximately 2.5 that of a Doppler base, the total resonance width (FWHM) Δ_{res} being about 35 MHz.

Qualitatively, a sharp increase in the absorption at the resonance profile centre can be simply explained as follows. When the laser radiation frequency is far from an average frequency of the two transitions, that is, $\delta_0/2\pi \gg \Delta_{res}$, the light beam propagating along the z axis and the counterpropagating beam interact with different velocity groups of atoms in the gas due to the linear Doppler effect. In each group, the conditions of coherent population trapping are satisfied, in which the most of atoms are pumped to a coherent superposition of levels 1 and 2 (see Fig. 1), and the absorption of the laser beams becomes minimal. It is a so called dark state related to a relatively small amplitude of the wide Doppler profile in Fig. 3. At $\delta_0/2\pi \approx \Delta_{res}$, that is, near the resonance curve centre, both beams interact with the same atoms in the gas. In this case, it is possible to choose such experimental conditions that a dark state in atoms will be absent. The destruction of the dark state sharply increases absorption in the resonance medium. This simple consideration explains the essence of the phenomenon observed; however, it does not give an estimate of its value (the resonance contrast). Actually, a high contrast of the nonlinear resonance is a result of several constructively interacting optical effects, which intensify each other. A thorough consideration of this effect (hypercontrast) requires consideration of the real energy level structure in the

atom (taking into account all magnetic sublevels), which is beyond the scope of the present work. Such a consideration is given in previous works on this subject [26, 27]. Note that physics of this phenomenon has much in common with the effects observed on resonances of electromagnetically induced transparency and absorption (EIT and EIA) in the field of counterpropagating laser beams in the two-frequency [35, 36] and single-frequency magneto-optical [37–39] configurations, where the two-photon (Raman) detuning is scanned instead of the optical frequency.

Figure 4 demonstrates the effect of oscillations of the nonlinear resonance amplitude as the mirror moves as mentioned above. One can see that with a shift of the mirror M (see Fig. 2), which forms the counterpropagating laser beam, the amplitude oscillates in a range of ~50% of the maximal value. The experimental points in Fig. 4 are well approximated by a sinusoidal function with the period of ~17 mm, which agrees with theory [26, 27].

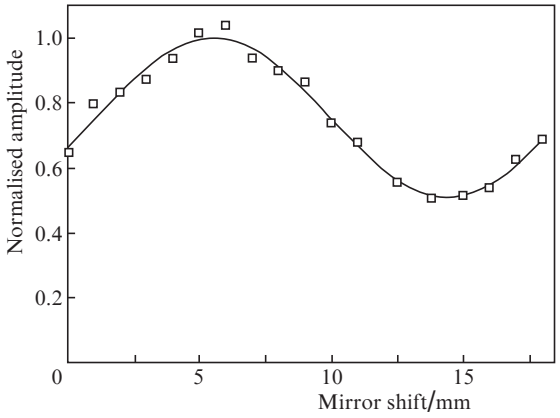

Figure 4. Amplitude oscillations of the sub-Doppler resonance normalised to the maximal value in the case of mirror displacement relative to a certain arbitrary initial position at $T \approx 50\,^{\circ}\mathrm{C}$, $P \approx 0.5$ mW. The curve is a harmonic approximation.

Dependence of the nonlinear resonance width Δ_{res}on total optical power P at the cell input is shown in Fig. 5. The beams in the experiments are narrow (~1 mm) and data presented in Fig. 5 refer to strong fields such that $I > I_{sat}$, where I_{sat} is the saturation intensity (~1 mW cm^{-2}). The dependence observed is typical for homogeneously broadened resonances in gases and can be approximated by a square root dependence $\sim(a + P)^{1/2}$, where a is a constant [34, 40]. Here, the resonance width weakly depends on the vapour temperature in the range of moderate (at most 50 °C) temperatures. This is related to the fact that at such temperatures, the optical density OD of the resonance medium is small: $\mathrm{OD} = \lg(P_{in}/P_{out}) \approx 0.1$ for the case of Fig. 3 (here, P_{in}, P_{out} are the radiation powers in the exact resonance conditions at the cell input and, correspondingly, after passing it forward and backward). In this case, the sub-Doppler resonance profile is close to Lorentzian and repeats the resonance profile $\alpha(\delta_0)$ for a single atom in the gas. As temperature increases, the concentration of resonant atoms also becomes greater and the medium becomes optically dense (OD ~ 1). This additionally broadens the nonlinear resonance, the profile of the latter can be qualitatively approximated by the dependence $\sim\exp[-n_a L\alpha(\delta_0)]$, where n_a

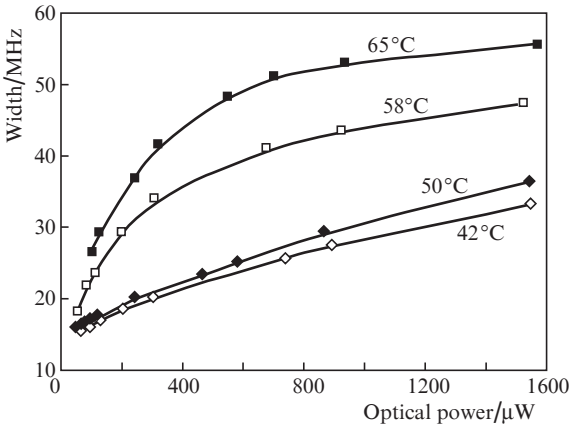

Figure 5. Total width of the sub-Doppler resonance vs. the optical power at the cell input at various temperatures of caesium vapours.

is the atomic concentration and L is the cell length. In our experiments at $T = 65\,^{\circ}\mathrm{C}$ and $P_{in} = 1.5$ mW the optical density measured at the resonance centre ($\delta_0 = 0$) is OD ≈ 0.7.

The resonance contrast is a very important parameter. It may be defined in several ways depending on a particular application. Let us introduce and analyse two contrast parameters of a nonlinear resonance with respect to the value of Doppler profile D (see Fig. 3) and to the background signal B [41]:

$$C_D = 100 \times A/D, \tag{1}$$

$$C_B = 100 \times A/B. \tag{2}$$

In Fig. 6a one can see that for contrast C_D a low vapour temperature is preferable, at which the absorption of a laser field far from the sub-Doppler resonance is small. In this case, contrast C_D may reach 250%, which, as noted in Introduction, is absolutely not typical for sub-Doppler resonances in many other observation configurations.

As for the parameter C_B (Fig. 6b), its dependence on the laser field power demonstrates a quick optimum; in addition, there is an optimal temperature as well. For example, for the optimal values one may choose $P \approx 300$ μW and $T \approx 60\,^{\circ}\mathrm{C}$. Both definitions of the sub-Doppler resonance contrast are important in the development of the QFS, namely: contrast C_D is mostly important when vapour fluorescence is analysed (see, for example, [15]), whereas C_B is needed when the transmitted signal is used, as in our case (see Fig. 2).

The main metrological characteristic of the QFS is the relative frequency stability, which conventionally is characterised by Allan deviation σ_y [1, 42]. In the quantum noise limit

$$\sigma_y \approx \frac{\Delta\nu/\nu_0}{\mathrm{SNR}}\frac{1}{\sqrt{\tau}}, \tag{3}$$

where $\Delta\nu$ is the resonance width in hertz (FWHM); $\nu_0 = \omega_0/2\pi$; and SNR is the signal-to-noise ratio (in the considered limit, $\mathrm{SNR} \approx A/\sqrt{B}$). Thus, a short-term frequency stability of the QFS is inversely proportional to the parameter that may be called the quality of reference resonance Q:

$$\sigma_y(\tau = 1\,\mathrm{c}) \sim \frac{1}{Q}, \quad Q = \frac{C_B/100\%}{\Delta\nu\sqrt{B}}. \tag{4}$$

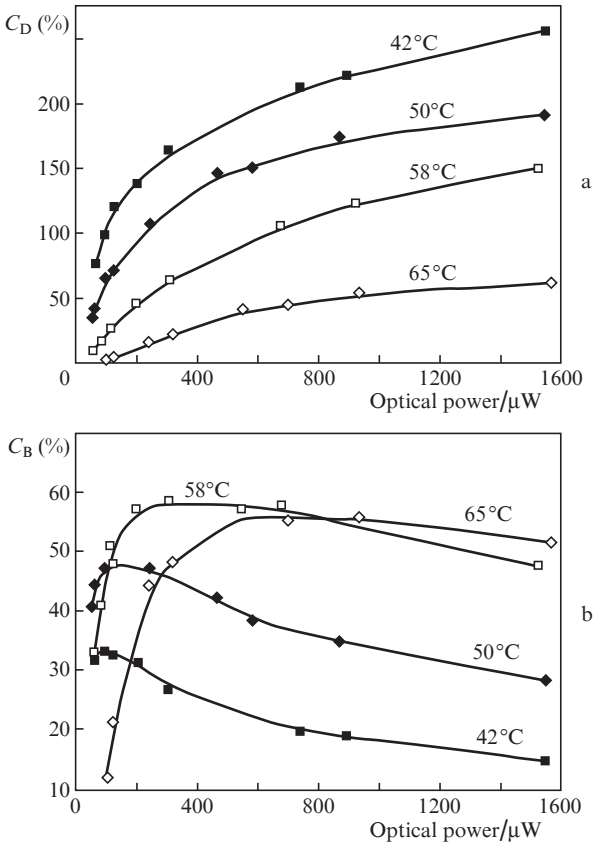

Figure 6. Dependences of the contrasts for (a) C_D and (b) C_B resonances determined by expressions (1) and (2) on the optical power and temperature of caesium vapours.

Hence, maximisation of the parameter Q is of primary importance for the employment of the two-frequency spectroscopy method in quantum metrology.

It follows from Fig. 7 that the same value of Q can be attained at various T and P combinations. Preferable should be the ranges of low temperatures and optical powers, which is due to the necessity of providing a low power consumption of the developed QFS's. Thus, for the optimal values it is reasonable to take $T \approx 50\,^{\circ}\mathrm{C}$ and $P \approx 0.5$ mW.

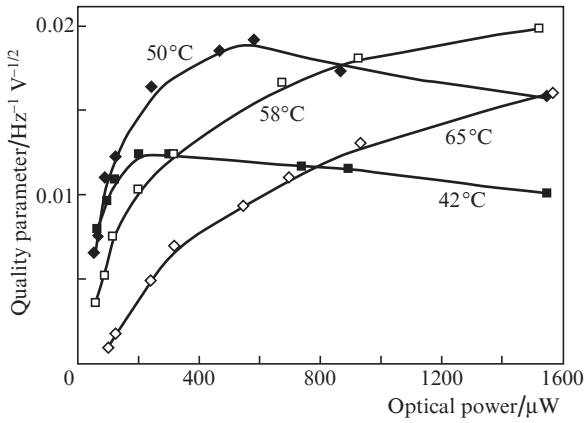

Figure 7. Dependences of the quality factor of nonlinear resonance on the optical power and cell temperature.

2.2. Pump–probe scheme

A schematic of an experimental setup shown in Fig. 8 is in many respects similar to that in Fig. 2. The difference is in the method of forming the counterpropagating laser beam. Now both beams are completely independent: the initial laser beam splits into two beams of equal power, which pass to a cell from the opposite ends. The beam optical powers are adjusted through the mutual orientation of the PBS and the output collimator of a fibre EOM. Despite of the apparent similarity of the two configurations, there is a principal difference, which may affect the parameters of the observed resonances. Obviously, in the scheme discussed in Section 2.1, an intensity of the counterpropagating beam directed against the z axis (see Fig. 2) depends on the degree of laser beam absorption along its first passage through the cell. In other words, the intensities of the counterpropagating beams in this scheme principally cannot be equal (at equal beam diameters). However, as was shown in [26, 27], the equality of intensities of the counterpropagating beams is the requirement for obtaining the maximal light absorption at the resonance centre (at $\delta_0 = 0$).

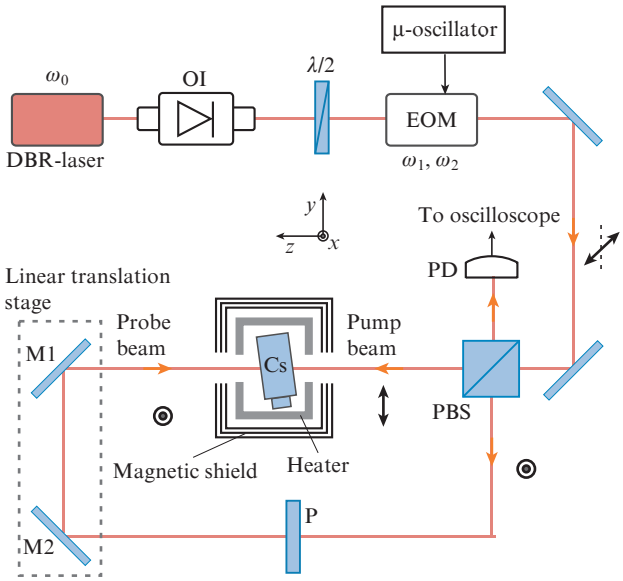

Figure 8. Experimental setup with the initial beam split to a pump beam and a probe beam; P is the polariser cutting off the pump radiation.

In the scheme with the splitting of the initial beam into two independent (pump and probe) beams, there is a possibility to make intensities of the counterpropagating beams equal. On the other hand, in the scheme with a single mirror (see Fig. 2), the beam, which absorption is analysed by a photodetector, passes a twice longer resonance medium and the absorption is also increased (as at the resonance centre so and far from it). In view of these facts, it is difficult to conclude *a priori* which scheme would be preferable for the employment in QFS's. Therefore, similarly to the scheme in Fig. 2, we will present measurement results for the sub-Doppler resonance parameters in the pump–probe scheme.

A high contrast of the sub-Doppler resonance is additionally illustrated in Fig. 9, where two resonance curves of the probe wave absorption are presented: with the pump wave

and without it. In the scheme considered (Fig. 8) apart from the previous variant (Fig. 2), the pump wave may be excluded, for example, by simply shutting the beam. By juxtaposing the two curves, one can select part of a resonance curve that is related to the simultaneous action of the two counterpropagating beams, that is, the central sub-Doppler resonance. It follows from Fig. 9 that at given experimental parameters the amplitude of the sub-Doppler resonance is approximately thrice that of the wide Doppler profile.

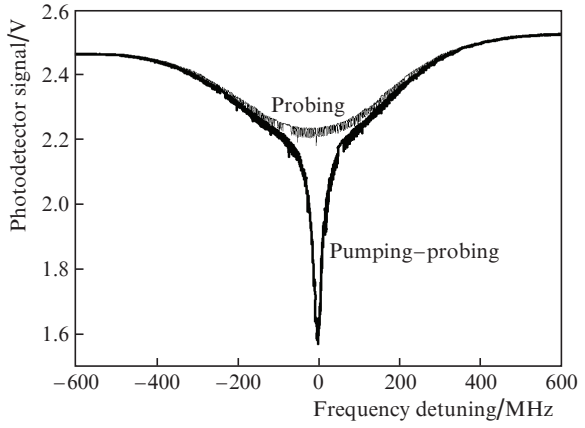

Figure 9. Resonance absorption of the probe wave with absent (probe) and present (pump–probe) pump wave at $T \approx 50\,^{\circ}\mathrm{C}$, $P \approx 1.3$ mW.

Figure 10 demonstrates the dependence of a sub-Doppler resonance on the total optical power. As in the scheme in Fig. 2, in the new scheme the nonlinear resonance is additionally broadened at elevated temperatures. Measurement results of the nonlinear resonance contrast are presented in Fig. 11. One can see that at equal intensities of the counterpropagating beams, contrast C_D may reach 450%, whereas in the previous scheme it was 250%. The parameter C_B (similarly to the case of the scheme in Fig. 2) has an optimum in the optical power; however, no extremum is observed in this case in the dependence on the cell temperature (in the range of temperatures considered).

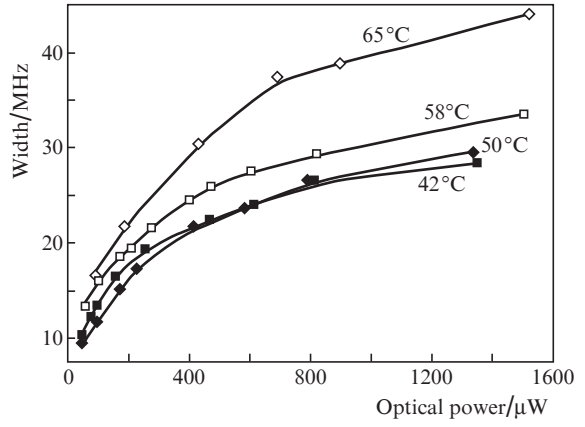

Figure 10. Total width of the sub-Doppler resonance vs. the optical power at various temperatures of caesium vapours in the pump–probe scheme.

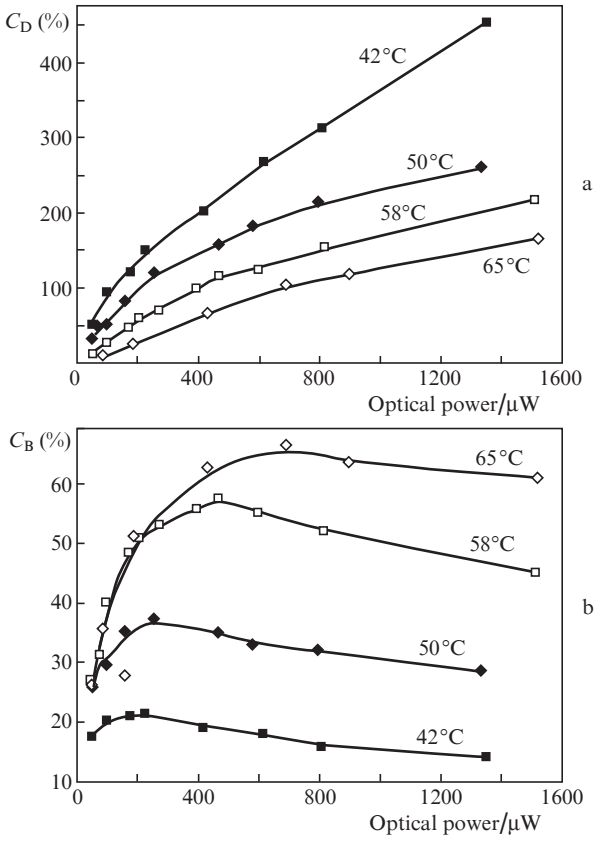

Figure 11. Dependences of the contrasts for (a) C_D and (b) C_B resonances determined by expressions (1) and (2) on the optical power and temperature of caesium vapours in the pump–probe scheme.

It follows from Fig. 12 that, in contrast to the scheme in Fig. 2, the quality parameter of nonlinear resonance has no extremum in the range of optical powers considered as well. However, it seems that the optimal cell temperature value becomes apparent. Thus, from the viewpoint of using the configuration considered for developing a QFS, the optimal values are $T \approx 60\,^{\circ}\mathrm{C}$ and $P \approx 1.5$ mW. In this case, approximately the same nonlinear resonance quality is obtained as in the scheme in Fig. 2 where the initial beam is not split into two beams. Nevertheless, a higher cell temperature and laser emis-

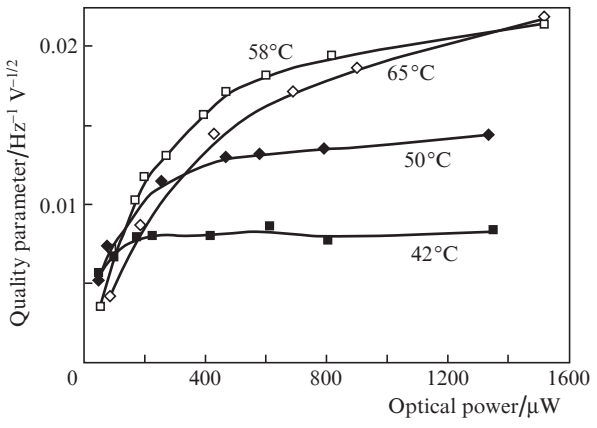

Figure 12. Quality parameter of the nonlinear resonance vs. the optical power and cell temperature in the pump–probe scheme.

sion power are required (as compared to $T \approx 50\,^{\circ}\mathrm{C}$ and $P \approx 0.5$ mW, see Fig. 7).

3. Comparison of the two-frequency and single-frequency methods for resonance excitation

In order to demonstrate advantages of the two-frequency spectroscopy method we may compare the observed resonance with a similar sub-Doppler resonance, obtained in the widely used single-frequency configuration. It can be realised on the same experimental setup as in Section 2.2 (Fig. 8), however, with the EOM switched off. In this case, the laser frequency ω_0 is adjusted in resonance with the transition $F_g = 3 \rightarrow F_e = 4$ where the sub-Doppler resonance has the highest contrast as compared to other dipole transitions of the D_1 line.

As follows from Fig. 13, the resonance of saturated absorption in the single-frequency method has a substantially lower amplitude than in the two-frequency method, the resonance width being much greater as well. The latter circumstance is related to the fact that the transition $F_g = 3 \rightarrow F_e = 4$ is open and that the most of the atoms are optically pumped to the nonresonance level $F_g = 4$, which additionally broadens the resonance [30]. In the two-frequency regime near the sub-Doppler resonance ($\delta_0 \approx \Delta_{res}$) these factors are absent.

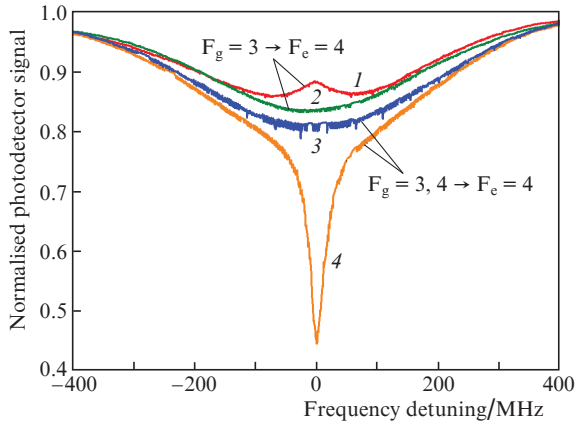

Figure 13. Resonance absorption of the probe wave in the case of a single-frequency regime with the pump wave (*1*), without it (*2*), and in the case of two-frequency regime without the counterpropagating beam (*3*) and with counterpropagating beam (*4*) at $T \approx 58\,^{\circ}\mathrm{C}$, $P \approx 1.5$ mW.

Quality parameters of nonlinear resonance obtained by different methods are shown in Fig. 14. In each case, the optimal temperature is chosen with the best Q value (in particular, in the single-frequency regime $T_{opt} \approx 58\,^{\circ}\mathrm{C}$). One can see that in the two-frequency method of observation, the parameter Q is substantially greater than in the case of the standard single-frequency approach. According to (4) it should result in the corresponding enhancement of the short-term stability of a QFS based on the two-frequency method.

4. Conclusions

Parameters of sub-Doppler resonances observed in caesium vapours are compared and discussed for different optical

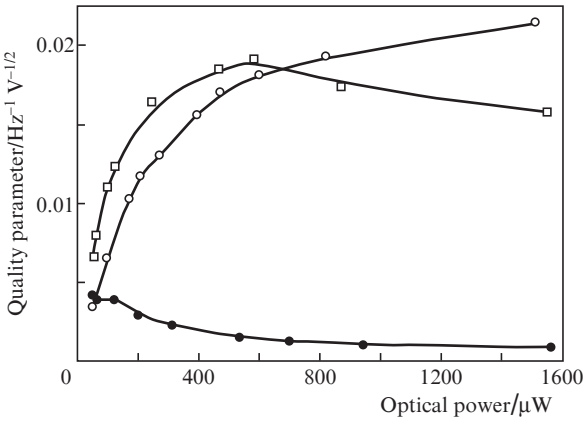

Figure 14. Quality parameter of the nonlinear resonance vs. the optical power in the two-frequency regime with the employment of mirror (▫), in the bichromatic regime with the splitting of the initial beam into the pump and probe beams (○), and in the single-frequency regime (●).

schemes with the employment of the two-frequency laser spectroscopy method that was recently suggested for developing a miniature QFS on their bases. In particular, in the two-frequency regime, two methods of forming the required laser field in a caesium cell have been experimentally studied: by reflecting the initial laser beam from a highly reflecting mirror back to the cell (with the turn of the linear polarisation by 90° in a quarter-wave plate) and by splitting the laser beam into two independent beams (the pump–probe scheme) possessing orthogonal linear polarisations. The main parameter in the comparison of nonlinear resonances was the quality parameter Q introduced according to formula (4), which substantially determines the QFS short-term stability. The investigations performed have shown that the first scheme with a single highly reflecting mirror (see Fig. 2) is preferable for the development of a miniature QFS based on the analysis of the laser beam passage through a resonance medium. In such a scheme, the maximal resonance quality is attained at a lower cell temperature and optical power as compared to the pump-probe scheme. In addition, the first scheme with a single mirror is simpler in realisation and adjustment and can be made more compact than the second one.

The possibilities of the two-frequency spectroscopy method are demonstrated by comparing it with the results of the widely used method based on a single-frequency configuration of the laser field, in which a conventional resonance of saturated absorption is observed in the form of a peak in the medium transmission signal. The data presented show that the two-frequency method is substantially better than the single-frequency approach from the viewpoint of attaining a high value of the quality parameter of nonlinear resonance. Note that, in addition to the short-term frequency stability (Allan deviation σ_y for 1 s), a long-term stability (σ_y at the averaging time of 10^3–10^5 s) is also important for the QFS. This stability, as a rule, is limited by the relatively slow drifts of an optical frequency, which are caused by various physical factors: fluctuations of a cell temperature, laser emission intensity, and so on. This problem requires a separate thorough study.

Acknowledgements. The work was supported by the Russian Science Foundation (Grant No. 17-72-20089). M.N. Skvortsov and I.S. Mesenzova are also grateful for the support of

the Russian Foundation for Basic Research (Grant No. 20-32-90029), which made it possible to fabricate a compact physical unit for performing experiments by the two-frequency method for caesium atom spectroscopy.

References

1. Riehle F. Frequency Standards: *Basics and Applications* (Weinheim: Wiley-VCH Verlag, 2004; Moscow: Fizmatlit, 2009).
2. The Event Horizon Telescope Collaboration et al. *Astrophys. J. Lett*., **875**, L1 (2019).
3. Cacciapuoti L., Salomon Ch. *Eur. Phys. J. Special Top.*, **172**, 57 (2009).
4. Roberts B.M., Blewitt G., Dailey C., Murphy M., Pospelov M., Rollings A., Sherman J., Williams W., Derevianko A. *Nat. Commun*., **8**, 1195 (2017).
5. Grotti J. et al. *Nat. Physics*, **14**, 437 (2018).
6. Goncharov A.N., Bonert A.E., Brazhnikov D.V., Shilov A.M., Bagaev S.N. *Quantum Electron*., **44**, 521 (2014) [*Kvantovaya Elektron*., **44**, 521 (2014)].
7. Ludlow A.D., Boyd M.M., Ye J., Peik E., Schmidt P.O. *Rev. Mod. Phys*., **87**, 637 (2015).
8. Taichenachev A.V., Yudin V.I., Bagaev S.N. *Phys. Usp*., **59**, 184 (2016) [*Usp. Fiz. Nauk*, **186**, 193 (2016)].
9. Hafele J., Keating R. *Science*, **177**, 166 (1972).
10. Takamoto M., Ushijima I., Ohmae N., Yahagi T., Kokado K., Shinkai H., Katori H. *Nat. Photonics*, **14**, 411 (2020).
11. Poli N., Schioppo M., Vogt S., Falke St., Sterr U., Lisdat Ch., Tino G.M. *Appl. Phys. B*, **117**, 1107 (2014).
12. Gubin M.A., Tyurikov D.A., Shelkovnikov A.S., Kovalchuk E.V., Kramer G., Lipphardt B. *IEEE J. Quantum Electron*., **31**, 2177 (1995).
13. Bagayev S.N., Dmitriyev A.K., Pokasov P.V. *Laser Phys*., **7**, 989 (1997).
14. Affolderbach C., Mileti G. *Rev. Sci. Instrum*., **76**, 073108 (2005).
15. Ignatovich S.M., Skvortsov M.N., Vishnyakov V.I., Brazhnikov D.V., Kvashnin N.L. *J. Phys. Conf. Ser*., **793**, 012010 (2017).
16. Alzetta A., Gozzini A., Moi L., Orriols G. *Nuovo Cimento B*, **36**, 5 (1976).
17. Zhang H. et al. *IEEE J. Solid-St. Circ*., **54**, 3135 (2019).
18. Vicarini R., Abdel Hafiz M., Maurice V., Passilly N., Kroemer E., Ribetto L., Gaff V., Gorecki C., Galliou S., Boudot R. *IEEE T. Ultrason. Ferr*., **66**, 1962 (2019).
19. Skvortsov M.N. et al. *Quantum Electron*., **50**, 576 (2020) [*Kvantovaya Elektron*., **50**, 576 (2020)].
20. Kitching J. *Appl. Phys. Rev*., **5**, 031302 (2018).
21. https://directory.eoportal.org/web/eoportal/satellite-missions/c-missions/chomptt.
22. Geiger R., Landragin A., Merlet S., Pereira Dos Santos F. *AVS Quantum Sci*., **2**, 024702 (2020).
23. Hummon M.T., Kang S., Bopp D.G., Li Q., Westly D.A., Kim S., Fredrick C., Diddams S.A., Srinivasan K., Aksyuk V., Kitching J.E. *Optica*, **5**, 443 (2018).
24. Maurice V., Newman Z.L., Dickerson S., Rivers M., Hsiao J., Greene P., Mescher M., Kitching J., Hummon M.T., Johnson C. *Opt. Express*, **28**, 24708 (2020).
25. Abdel Hafiz M., Coget G., De Clercq E., Boudot R. *Opt. Lett*., **41**, 2982 (2016).
26. Brazhnikov D., Petersen M., Coget G., Passilly N., Maurice V., Gorecki C., Boudot R. *Phys. Rev. A*, **99**, 062508 (2019).
27. Abdel Hafiz M., Brazhnikov D., Coget G., Taichenachev A., Yudin V., De Clercq E., Boudot R. *New J. Phys*., **19**, 073028 (2017).
28. Arimondo E., Orriols G. *Lett. Nuovo Cimento*, **17**, 333 (1976).
29. Pappas P.G., Burns M.M., Hinshelwood D.D., Feld M.S. *Phys. Rev. A*, **21**, 1955 (1980).
30. Vasil'ev V.V., Velichanskii V.L., Zibrov S.A., Sivak A.V., Brazhnikov D.V., Taichenachev A.V., Yudin V.I. *J. Exp. Theor. Phys*., **112**, 770 (2011) [*Zh. Exp. Teor. Fiz*., **139**, 883 (2011)].
31. Saprykin E.G., Chernenko A.A., Shalagin A.M. *J. Exp. Theor. Phys*., **119**, 196 (2014) [*Zh. Exp. Teor. Fiz*., **146**, 229 (2014)].
32. Brazhnikov D.V., Novokreshenov A.S., Ignatovich S.M., Taichenachev A.V., Yudin V.I. *Quantum Electron*., **46**, 453 (2016) [*Kvantovaya Elektron*., **46**, 453 (2016)].
33. Knappe S.A., Robinson H.G., Hollberg L. *Opt. Express*, **15**, 6293 (2007).
34. Sosa K., Oreggioni J., Failache H. *Rev. Sci. Instrum*., **91**, 083101 (2020).
35. Taichenachev A.V., Yudin V.I., Velichanskii V.L., Kargopol'tsev C.V., Wynands R., Kitching J., Hollberg L. *JETP Lett*., **80**, 236 (2004) [*Pis'ma Zh. Eksp. Teor. Fiz.*, **80**, 265 (2004)].
36. Brazhnikov D., Ignatovich S., Vishnyakov V., Boudot R., Skvortsov M. *Opt. Express*, **27**, 36034 (2019).
37. Brazhnikov D.V., Taichenachev A.V., Tumaikin A.M., Yudin V.I. *Laser Phys. Lett*., **11**, 125702 (2014).
38. Brazhnikov D.V., Ignatovich S.M., Vishnyakov V.I., Skvortsov M.N., Andreeva Ch., Entin V.M., Ryabtsev I.I. *Laser Phys. Lett*., **15**, 025701 (2018).
39. Brazhnikov D.V., Ignatovich S.M., Novokreshchenov A.S., Skvortsov M.N. *J. Phys. B: At. Mol. Opt*., **52**, 215002 (2019).
40. Letokhov V.S., Chebotayev V.P. *Nonlinear Laser Spectroscopy* (Berlin: Springer-Verlag, 1977; Moscow: Nauka, 1990)].
41. Shah V., Kitching J., in *Advances in Atomic, Molecular, and Optical Physics* (Elsevier Inc., 2010) Vol. 59, Ch. 2.
42. Vanier J., Audoin C. *The Quantum Physics of Atomic Frequency Standards* (Bristol and Philadelphia, 1989).